Proceedings of FED98
ASME/FED Third International Symposium on Numerical Methods for Multiphase Flow
June 21-26, 1998, Washington, DC, USA

FEDSM98-5027

COMPUTATION OF SHOCK WAVES IN CAVITATING FLOWS

Tim Colonius*
Christopher E. Brennen
Fabrizio d'Auria

Division of Engineering and Applied Science
California Institute of Technology
Pasadena, CA 91125
email: colonius@green.caltech.edu

ABSTRACT

Realistic cavitating flows are dominated by a large number of interacting bubbles. These clouds of bubbles exhibit highly nonlinear behavior with sudden changes in void fraction. Because of the potential damage caused by the coherent collapse of bubble clouds, there is a need for effective numerical models to predict their behavior. This paper presents a newly developed computational methodology to solve a continuum model of bubbly cavitating flow in which a Lagrangian finite volume technique is used to accurately and efficiently track all flow variables in space and time. We also present results for the solution of a one-dimensional model problem, namely cavitating shock waves produced by the normal motion of a wall bounding a semi-infinite domain of fluid. The roles of wave steepening and damping mechanisms in the collapse of bubble clouds are highlighted.

INTRODUCTION

The violent effects of the nonlinear dynamics of cavitation bubbles and clouds of such bubbles include intense noise radiation and material damage. Despite the negative consequences, neither quantitative nor qualitative prediction of these effects is presently possible for realistic cavitating flows.

The nonlinear growth and collapse of a single gas-phase bubble in a liquid has been widely investigated and different modes of bubble collapse near solid boundaries have been identified. However, the fluid dynamics associated with realistic cavitating flows is often dominated by interactions of a large number of bubbles. It has been proposed that such interactions, including the collapse of clusters of cavitation bubbles, are responsible for cavitation damage (Vyas & Preece 1974, Hansson & Mørch 1980, 1982, Mørch 1980). More recent work has catalogued some of the key phenomena associated with clouds of cavitation bubbles (d'Agostino & Brennen 1983, 1989, Smereka & Banerjee 1988, Omta 1992, van Wijngaarden & Buist 1992, Kumar & Brennen 1993b, 1993a, Wang 1996, Reisman 1997). For example the calculations of nonlinear bubble cloud dynamics by Wang and Brennen (1994, 1995, 1996) show clearly that the collapse of a cloud of bubbles involves the formation of a shock wave which, under certain circumstances, propagates inward through the cloud. Geometric focusing leads to very large local pressures and suggests the potential for severe noise and damage.

In this paper we present the details of a computational methodology which has been explicitly developed and refined for the purpose of accurately and efficiently computing bubbly cavitating flow. The highly nonlinear dynamics of clouds of cavitation bubbles can lead to a variety of difficulties with the numerical model. These include stiff-

*Address all correspondence to this author.

ness due to the very short time scale associated with violent collapse, Lagrangian tracking of the flow variables, the resolution of unsteady (propagating) shock waves, and the accurate modeling of damping mechanisms during the collapse of bubble clouds. In the next section we discuss the continuum modeling of clouds of cavitation bubbles, including the development of a new nonreflecting boundary condition which attempts to model the free space problem on a finite computational domain. The numerical method and its validation follow. As a first application we consider a transient problem in one spatial dimension, namely the cavitation caused by normal motion of a wall bounding a semi-infinite domain of fluid.

PHYSICAL MODELING

We consider a continuum bubbly flow model (d'Agostino & Brennen 1983, 1989, Biesheuvel & van Wijngaarden 1984). The equations and simplifying assumptions and their justification are briefly described here – Brennen (1995) should be consulted for more detailed discussion of the derivation.

Key assumptions present in the continuum model are that population of bubbles is fixed (neither fission nor fusion occur), the liquid phase is incompressible, variations in velocities and fluid properties occur on length scales large compared to the bubble size, and that the bubble nuclei are initially uniformly distributed in the flow. These assumptions lead to conservation equations for mass and momentum of the bubbly mixture:

$$\frac{D\rho}{Dt} + \rho\frac{\partial u_i}{\partial x_i} = 0, \tag{1}$$

$$\frac{Du_j}{Dt} + \frac{1}{\rho}\frac{\partial p}{\partial x_j} = 0. \tag{2}$$

Note that viscous terms and gravity have been neglected in the momentum equation. The typical bubble radius, $R(x,t)$, and therefore the void fraction, is governed by the Rayleigh-Plesset equation:

$$R\frac{D^2(R)}{Dt^2} + \frac{3}{2}\left(\frac{DR}{Dt}\right)^2 + \delta_D\frac{1}{R}\frac{DR}{Dt} + \frac{2}{\mathrm{We}}\left(R^{-1} - R^{-3\gamma}\right) + \frac{\sigma}{2}\left(1 - R^{-3\gamma}\right) + P = 0, \tag{3}$$

The system of equations is closed by noting that the assumptions above lead to a relation between the density and bubble radius:

$$\rho = \left(1 + \frac{\alpha_0 R^3}{1-\alpha_0}\right)^{-1} \tag{4}$$

In Equations (1) to (4) ρ is the mixture density made dimensionless by the constant liquid density, ρ_L. Lengths, x_i, and the bubble radius, R, are normalized by an equilibrium bubble radius R_0, the mixture velocity, u_i, is normalized by the bubble natural frequency, ω_0 times the equilibrium bubble radius, the pressure, P is measured relative to its equilibrium value, p_0, and normalized by $\rho_L r_0^2\omega_0^2$. Time, t, is normalized by $1/\omega_0$. Moreover, σ is the cavitation number, defined as $\frac{p_0-p_v}{\frac{1}{2}\rho_L r_0^2\omega_0^2}$, where p_v is the vapor pressure. The ratio of specific heats is γ. The effective damping for spherical bubbles is denoted by δ_D and is discussed in detail below. The Weber number is given by $\mathrm{We} = \frac{\rho_L r_0^3\omega_0^2}{S}$ where S is the (constant) surface tension. Finally, it has been assumed that any non-condensable gas in the bubbles undergoes isentropic compressions and expansions.

One result of the way in which the equations have been made dimensionless is that $R = 1$, $P = 0$, $u = 0$, and $\rho = 1-\alpha_0$ constitute a steady solution of equation (3), and this is referred to as bubble equilibrium. For a slight disturbance to this equilibrium state, bubbles will oscillate with their natural frequency, ω_0, given by the solution as:

$$\frac{2}{\mathrm{We}}(3\gamma - 1) + \frac{3\gamma\sigma}{2} = 1, \tag{5}$$

Since we typically consider $\mathrm{We} \gg 1$ and $\gamma = 1.4$, we obtain

$$\sigma \approx 0.47 \tag{6}$$

In the present work we begin by deriving a numerical method for one dimensional flow. We consider a semi-infinite region bounded by a flat moving wall. The boundary condition for the wall is that the fluid velocity normal to the wall is equal to the wall velocity. Below we specifically consider sinusoidal motion of the wall given by:

$$u_w(x_w,t) = A\sin\left(2\pi(t/T)\right). \tag{7}$$

This introduces two additional nondimensional parameters, the amplitude, A, and the period of wall oscillation,T.

Often a semi-infinite domain can be treated numerically, at least for incompressible flow problems, by mapping the infinite domain to a finite computational one. For compressible flow problems which involve acoustic waves which

propagate to infinity and decay only slowly (or not at all in the case of one-dimensional inviscid flow), domain mappings are problematic since the waves become more and more poorly resolved as they propagate through the highly stretched mesh near infinity. In these types of problems, therefore, the computational domain is usually truncated at a finite location, and an artificial boundary condition is imposed.

There is, of course, some ambiguity in posing such an artificial boundary condition, and it is necessary to make additional assumptions about the flow outside the region of interest. Considering the one-dimensional flow next to the vibrating wall, suppose that there is a finite region (slab) of fluid which initially has a certain concentration of bubble nuclei, and outside the slab there is pure liquid. If the liquid is treated as strictly incompressible, this is tantamount to placing a solid wall at the edge of the slab, since any one dimensional motion of the (initially quiescent) flow outside the slab would either violate the condition of incompressibility ($\frac{\partial u}{\partial x} = 0$) or cause infinite pressures.

However, real liquids have a small, but finite, compressibility, and this allows certain disturbances to pass through the interface between the bubbly slab of fluid and the pure liquid. If we prevent this transmission of acoustic waves to the pure liquid, then we will cause the bubbly layer to resonate (that is, standing waves will form by repeated reflections within the bubbly slab). This situation can be remedied, at least approximately, by posing a nonreflecting boundary condition at the edge of the bubbly slab. The basic idea of nonreflecting boundary conditions is that all the waves at the boundary are propagating out of the domain, and the boundary condition should eliminate any incoming waves.

For linear one dimensional hyperbolic (nondispersive) systems it is possible to pose a nonreflecting boundary condition by decomposing the solution into a set of decoupled (characteristic) waves. In the present nonlinear problem, we have the possibility of one-dimensional wave propagation, but the waves are dispersive. Small amplitude disturbances with frequency ω and wavenumber k will propagate at a speed

$$c = \omega/k = \pm\left(\frac{1}{3\alpha_0(1-\alpha_0)}\left(1-\omega^2-i\omega\delta_D\right)\right)^{\frac{1}{2}}. \qquad (8)$$

Equation (8) follows from the Fourier transform of the linearized versions of Equations (1) to (4) (e.g. Brennen 1995). Note that ω is normalized by ω_0, k is normalized by $1/r_0$ and c is normalized by $r_0\omega_0$.

Furthermore, for small amplitude disturbances, it can be shown that the Fourier amplitudes of the velocity and pressure, $\hat{u}$ and $\hat{p}$, respectively, are related by:

$$\hat{u} = Z(\omega)^{\pm}\hat{p}, \qquad (9)$$

where $Z(\omega)^{\pm}$ is the "acoustic impedance", given by

$$Z(\omega)^{\pm} = \pm(1-\alpha_0)c = \pm\left(\frac{(1-\alpha_0)}{3\alpha_0}\left(\omega_0^2 - 1 - i\omega\delta_D\right)\right)^{\frac{1}{2}}, \qquad (10)$$

where the positive and negative roots corresponds to right-going and left-going waves (and positive and negative phase velocities), respectively. Thus at one boundary of the domain, a nonreflecting boundary condition is:

$$\hat{p} = Z^{+}\hat{u} + \hat{p}_I, \qquad (11)$$

where we have added $\hat{p}_I$ to allow the possibility of arbitrarily specified incoming pressure disturbances. This equation is nonlocal in time since it contains the square root of the frequency. If the frequency is assumed to be small, then we can approximate equation (11) by:

$$p(x_N,t) = \rho_0 c_0 u(x_N,t) - \frac{\delta_D c_0}{2}\frac{\partial p}{\partial x}(x_N,t) + p_I, \qquad (12)$$

where $c_0 = \omega_0(\frac{1}{3\alpha_0(1-\alpha_0)})^{\frac{1}{2}}$.

NUMERICAL METHOD

Equations (1) through (4) are integrated using a one-dimensional Lagrangian finite volume scheme in which each control volume face moves at the local fluid velocity. The Lagrangian framework is convenient for two reasons: first it facilitates the application of the boundary condition at the moving wall, and secondly, it allows the Rayleigh-Plesset equation to be integrated (for a particular Lagrangian element) as an ordinary differential equation (ODE). The method discretely conserves both mass and momentum. Consider a one dimensional space divided into a collection of N control volumes. Integrating Equations (1) and (2) over the control volumes we obtain, for $j = 1, 2, \cdots, N-1$:

$$\frac{d}{dt}\int_{x_j}^{x_{j+1}} \rho dx = 0, \qquad (13)$$

$$\frac{d}{dt}\int_{x_j}^{x_{j+1}} \rho u dx = P_j - P_{j+1}, \qquad (14)$$

Equation (13) and equation (14) describe the rate of change of the total mass and momentum in the jth control volume. Each of the faces ($j = 1,2,\cdots,N$) of the control volume moves with the local fluid velocity and therefore

$$\frac{dx_j}{dt} = u_j, \tag{15}$$

where u_j is shorthand for $u(x_j(t),t)$. Also, equation (3) can be split into two first order equations at each face:

$$\frac{dR_jV_j}{dt} + G_j + P_j = 0, \tag{16}$$

$$\frac{dR_j}{dt} - V_j = 0, \tag{17}$$

where

$$G_j = \frac{V_j^2}{2} + \delta_D R_j^{-1} V_j + \frac{2}{\mathrm{We}}\left(R_j^{-1} - R_j^{-3k}\right) + \frac{\sigma}{2}\left(1 - R_j^{-3k}\right), \tag{18}$$

Finally, the density and bubble radius at the faces are related by:

$$\rho_j = \left(1 + \frac{\alpha_0 R_j^3}{1-\alpha_0}\right)^{-1} \tag{19}$$

To integrate this system of (as yet exact) equations, it remains to approximate the integrals in equations (13) and (14). A second-order approximation is used:

$$\int_{x_j}^{x_{j+1}} f\,dx = \frac{\Delta x_j}{2}\left(f_j + f_{j+1}\right) + O(\Delta^3), \tag{20}$$

where $\Delta x_j = x_{j+1} - x_j$, and where f is any of R_jV_j, R_j, or M_j.

Equations (13) to (19) are $6N-2$ ODEs for $6N$ unknowns (ρ_j, R_j,V_j,x_j,u_j, and P_j at the edges of the control volumes, $j = 1,2,\cdots,N$). Specifying two boundary conditions closes the system. At the moving solid wall the velocity u_1 is prescribed. The approximate nonreflecting boundary condition derived above (equation (12)) is applied at the other end of the computational domain.

These equations are solved in the Lagrangian coordinate system. Note that, depending on the solution, the control volumes could become very small or very large. If they become very large then the trapezoidal rule given in equation (20) may not be accurate. In that case it may be necessary to remesh the computation by interpolating the Lagrangian quantities back to a regular grid.

An interesting feature of the discretized equations is that an explicit time marching of the equations will not conserve mass precisely. For explicit time marching, Equations (15) and (17) give x_j and R_j at the new time level. Equation (19) then gives the density at the new time level, and so in general, Equation (13) cannot be satisfied at the new time level. This may be related to difficulties previous investigators have encountered in solving similar equations with explicit schemes – see, for example, Omta (1992) and Wang (1996).

For this reason (and the additional advantage of handling stiffness) an implicit time marching scheme is used. The method chosen is a Richardson extrapolation method based on the implicit Euler method. For a given time step, a series of predictions are made for the solution at the new time level based on different numbers of subdivisions of the time interval. The series of predictions is then used to extrapolated to the limit of zero time step, and to provide an error estimate for the integration. The overall time step is adjusted based on the number of subdivisions and the error estimate. The details of the scheme are as given by Hairer and Wanner (1996). Numerical experiments showed that the extrapolation method is much more efficient than first and second order implicit schemes.

The basic time advancement of the extrapolation method is the implicit Euler method. For an ODE given by:

$$\frac{df}{dt} = f', \tag{21}$$

the discrete form is:

$$f^{n+1} = f^n + hf'^{n+1}, \tag{22}$$

where h is the time step. Using this integration scheme on Equations (13) to (19) and going through the algebra, we can establish N equations of the form

$$F_j(R_{j-1}^{n+1}, R_j^{n+1}, R_{j+1}^{n+1}) = 0, \qquad j = 1,2,\cdots N, \tag{23}$$

which contain N unknowns, R_j^{n+1}, for $j = 1,2,\cdots,N$. In each equation F_j, various parameters of the problem also appear as well as the fields from previous time levels.

To solve the nonlinear equations we use Newton's method [1]. For a system of nonlinear equations, we iterate upon the equation:

$$\sum_{j=1}^{N} J_{jk}(\delta R_k) = -F_j, \tag{24}$$

First, F is evaluated with a guessed value of R_j^{n+1}. The Jacobian matrix $J_{jk} = \frac{\partial F_j}{\partial R_k}$ is found and the resulting system of linear equations is solved for δR_k. This correction is added to the guessed R_j^{n+1}, new values for F and J are computed and the procedure continues until F is reduced to near zero such that equations (23) are solved. In the present case, the matrix J is tridiagonal in form and so equation (24) is easily (and rapidly) solved.

Finally, the stability of the above numerical scheme was analyzed using the von Neumann method (e.g. Ferziger 1981) for the linearization of Equations (13) to (19) about the equilibrium flow ($R = 1$). The resulting ODE is, in the semi-discrete limit, inherently stable, and therefore A-Stable implicit schemes will also be stable. Note that the extrapolated schemes used here are not A-Stable, but only nearly so, and they can be unstable for eigenvalues which lie very near the imaginary axis (Hairer & Wanner 1996). In practice we have found that our scheme is stable even for very large time steps, and even in the presence of significant nonlinearity.

CODE VALIDATION

Steadily propagating bubbly shock waves are one of the few fully nonlinear solutions of the governing one-dimensional equations of bubbly flow. We instigate a shock wave in the computational domain by specifying a fairly large amplitude pressure increase at the left boundary, in the form of an incident wave whose pressure is given by:

$$p_I = \frac{p_A}{2}\left(1 + \tanh\left(\frac{t}{T_f}\right)\right), \tag{25}$$

The parameter T_f controls the timescale over which the pressure jump is accomplished. The pressure rise begins propagating to the left through the domain at the "sonic speed," c, given above in equation (8). As it propagates, nonlinearity cause the wavefront to steepen and accelerate, and eventually a bubbly shock wave is formed. It eventually propagates to the left at a (constant) speed, u_1. To test the accuracy of the code, we compare in figure 1 the shock wave structure from the present unsteady code with the steady bubbly shock wave solution obtained by solving Equation 6.72 of Brennen (1995). Note that the steady equation is an ODE which must also be solved numerically and requires an initial position and rate of change of bubble radius with position which are taken from the unsteady numerical solution. The figures show excellent agreement between the two independent solutions. Apparently as the resolution of the unsteady solution is increased, the phase error between the two solutions is decreased. There is a slightly exaggerated decay of the subsequent rebounds and collapses in the numerical solution due to numerical dissipation. It should be noted that the present unsteady shock has propagated a substantial distance by the time the comparison is made. One would expect further dissipation of the collapses and rebounds to take place upon further propagation.

TEST OF NONREFLECTING BOUNDARY CONDITION

A series of computations were also performed to test the efficacy of the nonreflecting boundary condition. An incoming wave was generated at the nonreflecting boundary by specifying:

$$p_I = p_A \exp\left(-(t/T)^2\right), \tag{26}$$

If T is large enough, the energy of the wave is restricted to low frequencies, and, for small amplitude, it should propagate nondispersively at a speed, c, given by equation (8). The wave propagates first in the negative x direction, reflects from the solid wall, propagates in the positive x direction and eventually passes through the nonreflecting boundary. Because the boundary condition is approximate, some fraction of the wave energy is reflected back, and the process continues until there is no energy (or rather until there is nothing but accumulated numerical error) left in the domain. A measure of the efficacy of the boundary condition is the history of total "acoustic energy" which is estimated simply as $E(t) = \sum_{j=1}^{N} p_j^2$. Tests show that for very small amplitude ($p_A = O(10^{-3})$ and smaller) the reflection coefficient (ratio of energy in the domain before and after passage of the pulse through the boundary) is about 0.0016%. As the amplitude is increased the reflection coefficient increases owing to nonlinear effects which are not accounted for in the analysis. However, for p_A as large as 0.05 the reflection coefficient increases only to 0.36%, and clearly most of the energy is still absorbed by the boundary. Note that for these large amplitude disturbances the incident wave steep-

[1] Though in practice we find that just one Newton iteration per time step is most efficient when combined with the extrapolation procedure outlined above.

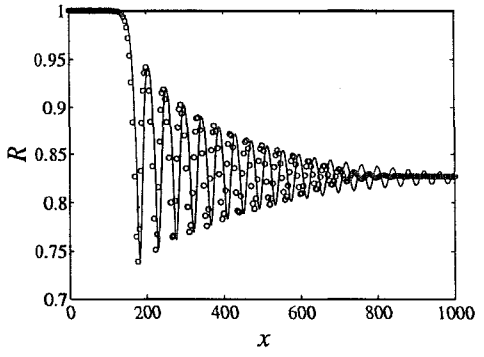

(a) $\Delta x = 4$

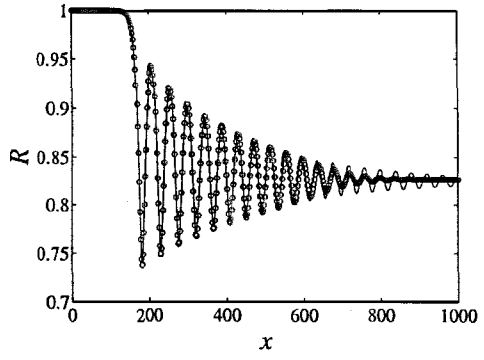

(b) $\Delta x = 2$

Figure 1. Comparison of numerically calculated unsteady (but propagating at a constant speed) shock wave and a steady shock given by the solution of Equation 6.72 of Brennen (1995). The bubble radius and distance are made nondimensional with the upstream equilibrium bubble radius. The various parameters (made nondimensional as discussed above) are are: We $= 1870$, $\delta_D = 0.04$, $\alpha_0 = 0.01$, $t_0 = 100$, $T_f = 25$, $\sigma = 0.475$, $k = 1.4$ ($\omega_0 = 1$). (a) Δx_j is initially 4 for each cell; (b) Δx_j is initially 2. These values do not change significantly during the course of the shock propagation.

ens and forms a bubbly shock, similar to that described in the previous section.

CLOUD CAVITATION NEAR A VIBRATING WALL

As an application of the newly developed numerical method, we consider the normal vibration of a wall adjacent to a semi-infinite fluid. For brevity, we consider here only a subresonant case in which the frequency of oscillation of the wall is one tenth of bubble natural frequency (in the undisturbed flow), $T = \frac{20\pi}{\omega_0}$. In what follows, the Weber number is taken to be large, and effective damping coefficient, δ_D is set to 0.4. The effects of damping are discussed in more detail in the next section. A more complete analysis of the present problem, including the resonant and superresonant cases will be given later (Brennen, Colonius & d'Auria 1997). The present configuration was studied by Kumar & Brennen (1993a) using weakly nonlinear analysis.

For small enough amplitudes, nonlinear effects are absent and, since the frequency is low, the phase speed of pressure disturbances is real according to equation (8). That is, wall vibration generates propagating disturbances (acoustic waves) which are only slightly attenuated by the viscosity. For higher frequency the phase speed in equation (8) becomes imaginary and disturbances die off exponentially with increasing distance from the wall.

As the amplitude is increased, two different nonlinear phenomena are manifest in the results. The first is a steepening of wavefronts similar to that in gasdynamics. This process is shown in figure 2, where the wall velocity is plotted along with the particle velocity some distance from the wall for several different amplitudes of wall motion. Note that the particle velocities are normalized by the maximum wall velocity in each case, and the results shown are those after an initial transient response has died out. For small amplitudes, linear behavior is observed, with a slight attenuation of the acoustic waves due to viscosity. For larger amplitude vibration, the compressions steepen into shocks.

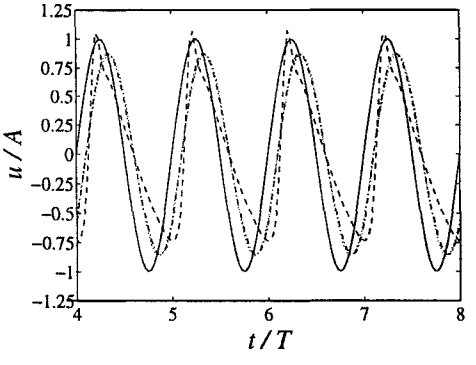

Figure 2. Nonlinear steepening of the waves. We $= 1870$, $\delta_D = 0.4$, $\alpha_0 = 0.01$, $\sigma = 0.475$. A grid of 801 points is used on a domain 400 units wide (relative to the initial equilibrium bubble radius). Plotted are: The wall velocity (———), the particle velocity at $x = 400$ for $A = 0.0001$ (·····), $A = 0.001$ (—·—), and $A = 0.01$ (----). All velocities are normalized by the amplitude of the wall velocity, A.

As the amplitude is further increased, an interesting saturation takes place and the amplitude of the asymptotic shock wave which is formed becomes independent of the amplitude of the wall vibration. This is illustrated in Figure 3 which shows results similar to Figure 2, but with higher

amplitude. Note that the particle velocity is not normalized by A in Figure 3. Unlike a gasynamic shock, there are secondary rebounds and collapses associated with the shock front.

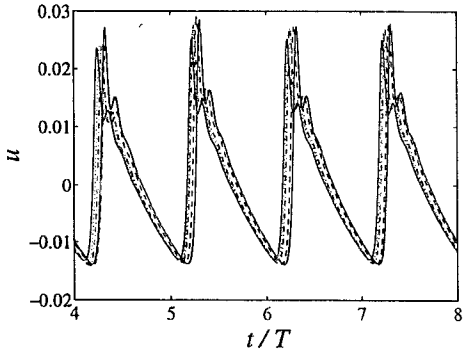

Figure 3. Asymptotic shock structure. Same parameters as figure 2 but with $A = 0.05$ (———), $A = 0.075$ (·····), $A = 0.01$ (—·—), and $A = 0.2$ (----), and $A = 0.3$ (———). Note that the velocities are not normalized by A.

In this latter regime cavitation is taking place near the wall and bubbles are growing significantly during the expansion phase of the motion. The maximum bubble size is still a strong function of the amplitude of the wall motion, despite the saturation of the asymptotic shock wave. The violent growth and collapse of the bubbles near the wall is shown in figure 4 where the bubble radius is plotted at the wall for the same set of amplitudes plotted in Figure 3.

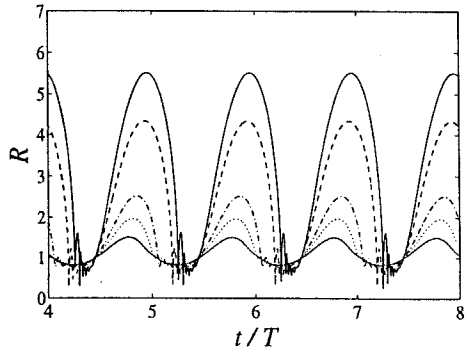

Figure 4. Growth and collapse of bubble radius near wall. Same parameters and legend as figure 3.

An hypothesis for the saturation of the asymptotic waveform is that for sufficiently large wall motion, the bubble radius grows large enough such that the "equilibrium" sound speed given by equation (8) is no longer relevant, but instead the local bubble natural frequency inside the cloud is greatly reduced. Thus the wall motion is no longer "subresonant" compared with local cloud conditions. The waves are "cut-off" (their phase speed becomes complex) and the wave decays exponentially with increasing distance from the wall. Upon collapse of the cloud the waves are then "cut-on" and a shock wave is formed. A similar "cut-off" phenomenon was observed in the results of Smereka & Banerjee (1988).

DAMPING MECHANISMS

It is appropriate to comment briefly on the various issues involved in choosing the magnitude of the damping parameter, δ_D, in the Rayleigh-Plesset equation (3). It has been recognized for many years, that several different physical processes may contribute to the dissipation of the volume oscillations of spherical bubbles. Chapman & Plesset (1971) provided a useful summary of the relative magnitudes of the contributions from viscous liquid effects, from acoustic radiation and from thermal effects. These are often approximated by a total "effective" viscosity for use in the damping term in the Rayleigh-Plesset equation. It is most often compared with experimental results for the attenuation of small amplitude acoustic waves though with mixed results (van Wijngaarden 1972). Even when these three contributions are taken into account, the result is sometimes orders of magnitude smaller than the observed attenuation.

Another mismatch is the number of collapses and rebounds observed for a cavitation bubble. Estimates of the spherical bubble damping (from all sources) lead to far larger and more numerous rebounds than are actually observed. It seems likely that the fission of the real bubbles which occurs in the first collapse, introduces additional dissipation mechanisms which greatly increase attenuation and reduce the number and magnitude of the rebounds which the resulting bubble cloud exhibits. Quantifying this additional (and dominant) attenuation mechanism presents a real challenge as yet not met.

In calculations of bubble cloud dynamics this issue becomes critical for several reasons. First and most obvious, the series of collapses and rebounds produced by each bubble will influence all of the other bubbles and therefore the coherent dynamics of the cloud. But, in addition, the complex shock structure which they produce has important consequences for the numerics which are required to resolve this structure, not only in the present one-dimensional calculations but, even more demandingly, in future multidimensional computations.

For the results presented in the last section we have used $\delta_D = 0.4$. Values of δ_D as large as 0.5 have been used to match theoretical and experimental predictions for the attenuation of acoustic waves in bubbly mixtures (van Wijngaarden 1972). Interestingly, it turns out that $\delta_D \approx 0.5$ represents a significant transition in the results presented in the last section. In Figure 5 the bubble radius at the wall is plotted over one period for a series of runs with $A = 0.3$ but with differing values of δ_D. For δ_D greater than 0.8 the maximum bubble radius begins to decrease significantly. For this large value of the damping there is no violent collapse and rebound of the cloud. For values below 0.8 the maximum bubble radius appears to saturate, and the primary difference in the results is the number of collapses and rebounds during each cycle. For values of δ_D less than 0.4 (not shown in the plot), the larger number of rebounds lead to greater computational requirements for adequate resolution of both temporal and spatial features of the flow. For values significantly lower than 0.4 we have not been able to obtain converged solutions. We conclude that there exists a value of the damping which not only avoids significant computational difficulties but also produces realistic results. For the present computation this critical value of damping $\delta_D = 0.4$, but we must note that its sensitivity to the other parameters (α_0, A, and T) has not yet been investigated in detail.

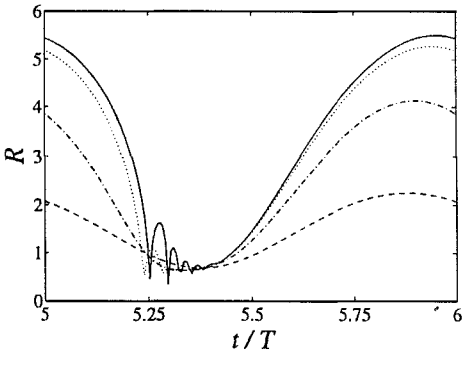

Figure 5. Growth and collapse of bubble radius near wall for $A = 0.3$ and $\delta_D = 0.4$ (———), $\delta_D = 0.8$ (·····), $\delta_D = 4.0$ (—·—), and $\delta_D = 40.0$ (----).

CONCLUSION

An efficient and accurate numerical method has been developed for computing one-dimensional cavitating flows. The flow adjacent to a vibrating wall (an idealized vibratory cavitation damage device) has been investigated for frequencies much smaller than the bubble natural frequency. Several interesting nonlinear phenomena are evident in the results. For sufficiently large amplitude, wave steepening leads to the formation of shocks However, as the amplitude is increased beyond a certain threshold, the strength of the propagating shock wave saturates, and the ever more violent cloud growth and collapse is limited to a region very near the wall.

Resonant and super-resonant vibration of the wall leads to other nonlinear phenomena including period doublings of the cloud growth and collapse cycle near the wall. These results will be presented later (Brennen et al. 1997). Eventually efficient numerical methods now need to be extended to multidimensional cavitating flows.

ACKNOWLEDGMENT

This research was supported, in part, by the Office of Naval Research under grant number N00014-91-J-1295. The third author is also grateful for support from the European Space Agency.

REFERENCES

Biesheuvel, A. & van Wijngaarden, L. (1984), 'Two phase flow equations for a dilute dispersion of gas bubbles in liquid', J. Fluid Mech. 148, 301–318.

Brennen, C. (1995), Cavitation and Bubble Dynamics, Oxford University Press.

Brennen, C., Colonius, T. & d'Auria, F. (1997), Computing shock waves in cloud cavitation, to be presented at the Third International Symposium on Cavitation, Gernoble, France, April 7-10, 1998.

Chapman, R. & Plesset, M. (1971), 'Oscillations of a cloud of bubbles of small and not so mall amplitude', ASME J. Basic Eng. 93, 373–376.

d'Agostino, L. & Brennen, C. (1983), On the acoustical dynamics of bubble clouds, in 'ASME CAvitation and Multiphase Flow Forum', pp. 72–75.

d'Agostino, L. & Brennen, C. (1989), 'Linearized dynamics of spherical bubble clouds', J. Fluid Mech. 199, 155–176.

Ferziger, J. (1981), Numerical Methods for Engineering Application, John Wiley & Sons.

Hairer, E. & Wanner, G. (1996), Solving Ordinary Differential Equations II, rev edn, Springer.

Hansson, I. & Mørch, K. (1980), 'The dynamics of cavity clusters in ultrasonic (vibratory) cavitation erosion', J. Appl. Phys. 51, 4651–4658.

Hansson, I., Kedrinskii, V. & Mørch, K. (1982), 'On the dynamics of cavity clusters', J. Phys. D 15, 1725–1734.

Kumar, S. & Brennen, C. (1993a), 'Some nonlinear interactive effects in bubbly clouds', J. Fluid Mech. 253, 565–591.

Kumar, S. & Brennen, C. (1993b), 'A study of pressure pulses generated by travelling bubble cavitation', J. Fluid Mech. 255, 541–564.

Mørch, K. (1980), On the collapse of cavity cluster in flow cavitation, in 'Springer Series in Electrophysics', Vol. 4, p. 95.

Omta, R. (1992), 'Oscillations of a cloud of bubbles of small and not so mall amplitude', J. Acoust. Soc. Am 82(3), 1018–1033.

Reisman, G. (1997), Dynamics, Acoustics and Control of Cloud Cavitation on Hydrofoils, PhD thesis, California Institute of Technology.

Smereka, P. & Banerjee, S. (1988), 'The dynamics of periodically driven bubble clouds', Phys. Fluids 31, 3519–3531.

van Wijngaarden, L. (1972), 'One-dimensional flow of liquids containing small gas bubbles', Ann. Rev. Fluid Mech. 4, 369–396.

van Wijngaarden, L. & Buist, J. (1992), 'The emission of sound by statistically homogeneous bubble layers', J. of Eng. Math. 26, 195–210.

Vyas, B. & Preece, C. (1974), Spec. tech. publ. 567, Technical report, Am. Soc. Test. Mater.

Wang, Y.-C. (1996), Shock Waves in Bubbly Cavitating Flows, PhD thesis, California Institute of Technology.

Wang, Y.-C. & Brennen, C. (1994), Shock wave development on the collapse of a cloud of bubbles, in 'Cavitation and Multiphase Flow Forum', Vol. FED 194, ASME, p. 15.

Wang, Y.-C. & Brennen, C. (1995), The noise generated by the collapse of a cloud of cavitation bubbles, in 'ASME/JSME Symposium on Cavitation and Gas-Liquid Flow in Fluid Machinery and Devices', Vol. FED 226, ASME, p. 17.